Chapter 4

Facile hydrogen evolution reaction on polypyrrole/NASICON (PPy/NFS) composites modified electrodes

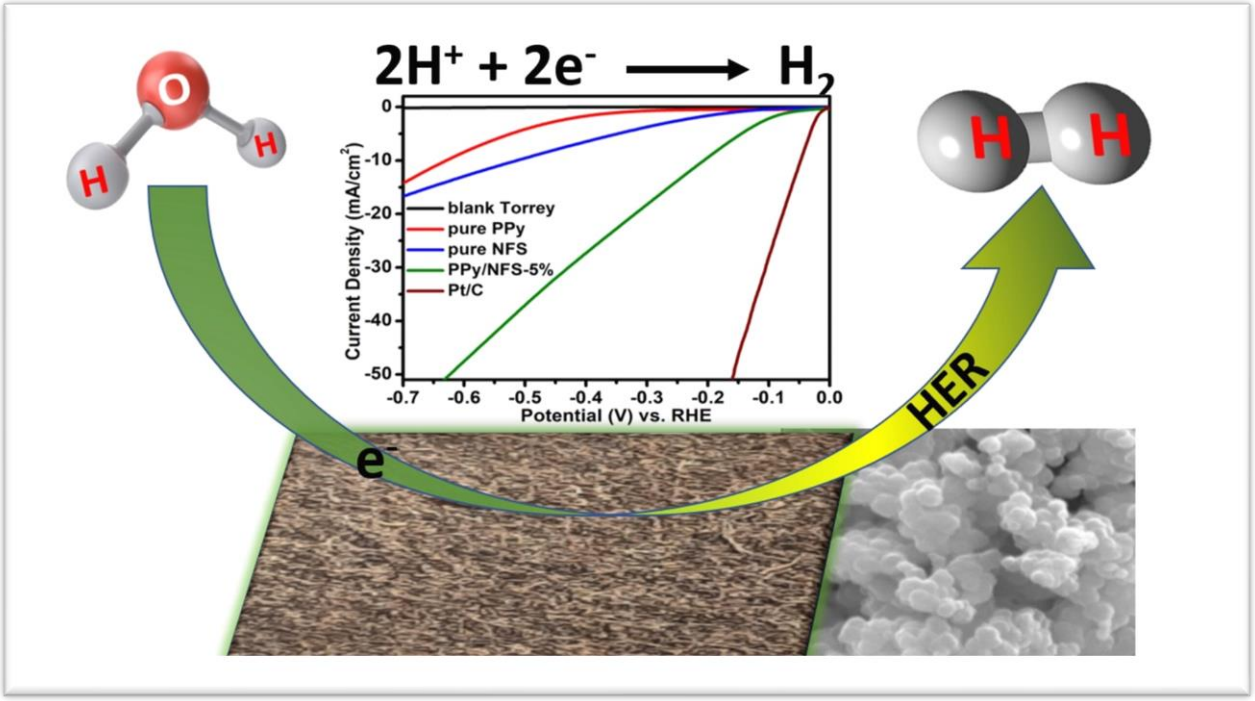

This chapter deals with the HER properties of nanocomposites of polypyrrole and NASICON-structured NFS (PPy/NFS) synthesized using various weight % of NFS immobilized into a fixed amount of PPy matrix at the monomeric level. The optimized PPy/NFS composites ratio offers high catalytic activity and stability towards HER to explore the alternatives of Pt-based HER catalysts.

4.1 Introduction

The continual and ever-increasing consumption of fossil fuels results in a slew of critical issues, including severe environmental contamination and a near-term lack of conventional fossil fuels [149]. Because global energy demand is expected to climb to roughly 27 TW in 2040, the consumption rate of fossil fuels will skyrocket, causing more CO_2 to accumulate in the atmosphere [150]. Although fossil fuels, including petroleum and natural gases, can still provide energy demand globally in the upcoming decades, their hazardous effect on environments and climates and limited reserves cannot fulfill future development goals [150]. To overcome these serious issues, we must introduce a renewable and clean energy system alternative to solve existing environmental pollution problems while addressing energy shortage problems [149], [150]. For this reason, countries worldwide have invested considerable effort toward producing renewable and carbon-free energy sources such as tidal, wind, geothermal, hydroelectric power, and solar energies [150], [151]. Despite their merits of being environmentally friendly, intermittent nature due to weather and time-dependent, low energy delivery efficiency, location specificity, and expensive maintenance limits their uses globally [151]. Therefore, it is essential to use other promising alternatives to address these problems. Hydrogen (H_2) is a good candidate for energy carriers due to its unique characteristics of maximum gravimetric and volumetric energy densities with carbon-free features, making it a suitable candidate for changing the energy structure demand globally in the future [60], [149]. It can be used as a fuel alternative to traditional fossil fuels and stored as extra energy using a system that interfaces with the renewable energy system for electricity. H_2 can be produced from different sources, such as biomass, coal, natural gas, petroleum, and water [151]. In the present scenario, it is mainly produced from natural gas and petroleum, which releases carbon dioxide as an undesired byproduct. Although biomass is a renewable resource, it cannot meet

large-scale energy demands. Hence, environmentally friendly and highly efficient techniques are required to produce clean and cost-effective hydrogens. In this regard, photoelectrochemical [152] and electrochemical water splitting techniques[153] are the most promising approaches, as they rely on unrestricted water sources with the capability of massive high-purity H_2 production. However, electrochemical water splitting is more tempting than photoelectrochemical in terms of higher flexibility and production efficiency[150].

The best catalyst available for electrochemical HER is noble-metal-based materials (Pt and Pt-based) [154], but exorbitant prices and scarce reserves limit their broad applicability. Many research groups worldwide are putting considerable effort into improving the noble-metal-based catalyst's consumption efficiency and exploring alternatives like earth-abundant catalysts with high efficiency and cost-effectiveness[60], [150]. Many metals [155], bimetals [155] and their compounds, including oxides[149], phosphides [155], [156], sulfides [60], tellurides [157], carbides [60], [155], nitride [155], metal alloy [155], and carbon-derived materials such as graphene oxides [158] and carbon nanotubes [159] have been reported till now to show activity towards HER with high efficiency. Nevertheless, electrode materials based on metals, bimetals, alloys, and metal oxides become inactive towards HER after a limited use due to metallic corrosion in harsh conditions like an acidic and basic medium [160]. To get around these restrictions, different composites of these materials were synthesized for electrocatalytic hydrogen evolution reactions, which have the advantages of being economical, noble, and toxic metal-free, environmentally friendly, and having extremely high stability. Conducting polymer-based nanocomposites with metals, bimetals, and their compounds emerged as one of the promising candidates for HER in recent years due to the vibrant superiority of compositional and morphological flexibilities, easy synthesis, and tunable diversity [161], [162], [163], [164]. Conducting polymer-based composite materials also has advantages concerning cost-

effectiveness, processibility, environmentally friendly and non-toxic nature [161], [162], [163], [164], [165]. Due to the synergistic effects of the polymer matrix and the nanofiller, CP-based nanocomposites are made conductive by combining a polymer matrix with nanofillers which exhibit excellent catalytic activity toward HER. Conducting polymers that have been explored for HER are polyaniline [165], polythiophene [166], Polyindole [167], poly-o-aminophenol [167], polypyrrole [164], [167], poly(3,4-ethylenedioxythiophene) (PEDOT) [168] including their composites [162], [164], [166]. Polypyrrole (PPy) is a high-potential material for energy conversion and storage [169]. However, the surface of PPy is comparatively hydrophobic and will hinder water adsorption, which will momentarily lead to poor HER catalytic performance [170]. NASICON-structured $Na_3Fe_2(SO_4)_2(PO_4)$ (hereafter termed as NFS), on the other side, has a much high affinity toward the water and can easily incorporate with the PPy matrix. The nitrogen in the PPy ring can easily interact with the metal center [164], [167], [170]. Due to the conjugation in PPy moieties, the electron sharing capability is enhanced from electron-rich nitrogen for PPy to NFS, which facilitates better charge transfer. Also, the PPy backbone contains positive charge centers, which enhance the charge transfer by interacting with the electron-rich centers.

In this chapter, noble-metal-free PPy/NFS composites have been synthesized via in-situ polymerization. We incorporated different weight percentages of nano NFS in fixed amounts of Pyrrole monomers in an aqueous solution, and ammonium persulphate was used as an oxidizing agent. The as-synthesized composites with different NFS weight percentages are denoted as PPy/NFS-2%, PPy/NFS-5%, PPy/NFS-10%, PPy/NFS-15%, and PPy/NFS-20%. The XRD, FTIR, TGA, XPS, SEM, and TEM techniques were used to characterize the as-prepared composite materials for structural, compositional, and morphological illustrations. These composites were then investigated for electrochemical Hydrogen Evolution Reaction.

Further, the composite material, which shows the best catalytic activity, pure PPy, and NFS, is investigated for the specific surface area using BET. In a highly acidic medium, PPy/NFS-5% (optimal ratio) showed good HER activity, with a remarkably lower onset potential of -26 mV and a lower Tafel slope of 101 mV dec^{-1}, as well as a relatively small overpotential of -206 mV associated to the current density of 10 mA/cm^2. The as-synthesized PPy/NFS-5% nanocomposites also presented long-term stability and good durability.

4.2 Experimental section

Chemicals

Pyrrole C_4H_5N (assay ≥98%), ammonium persulphate $(NH_4)_2S_2O_8$ (assay ≥98%), Mohr's salt $(NH_4)_2Fe(SO_4)_2(H_2O)_6$ (assay ≥ 99%), sodium hydrogen phosphate Na_2HPO_4 (assay ≥99%), and sodium carbonate Na_2CO_3 (assay ≥99.5%) were bought from Sigma Aldrich. All the chemicals (except pyrrole) were utilized as they were supplied, with no further purification required.

Synthesis of NFS

The synthesis of NFS was done by a simple chemical method as follows [171]: first, we dissolved 7.92 g of Mohr's salt in 100 mL DI water and stirred it for 1 hour at temp 90 °C. Then, 1.58 g of sodium hydrogen phosphate was supplied to the above solution with continuous stirring for 2 hours for proper mixing. After that, 1.07 g of sodium carbonate was mixed into the above solution mixture, causing spontaneous CO_2 evolution. The pH of the reaction mixture was kept basic by adding ammonia solution to precipitate, followed by calcination of as-prepared dried yellow powder at 500 °C for 12 hours in a muffle furnace (heating rate was maintained at 5 °C per min) to get the final crystalline NFS.

Synthesis of PPy/NFS composites

A facile chemical route was used to synthesize PPy/NFS composites. First, a fixed amount of pyrrole (0.5 ml) was transferred to a stoppered conical flask containing 70 ml of distilled water in ice-cold condition under continuous stirring. After that, the as-synthesized nano NFS (of different weight percentages) was also transferred to the above reaction mixture, and the stirring was continued for 2 hours for proper dispersion and interaction of pyrrole (Py) and NFS. After this, 30 ml of APS (100 mM) solution was added to the Py/NFS reaction mixture slowly and dropwise under continuous stirring conditions for polymerization. The stirring continued for another 2 hours after adding APS, followed by keeping the reaction mixture undisturbed for 24 hours to complete the remaining polymerization reaction. The following day, it was filtered and washed with DI water and ethanol to eliminate unreacted monomers. After that, the polymer composites were dried for 24 hours at 50 °C before using as an active material for electrochemical measurements.

Electrode fabrication:

First, a slurry ink was prepared by dispersing 4 mg of electrode materials in 1 mL of an ethanol-water mixture (2:3 V/V). It was then ultra-sonicated for 2 hours to exfoliate it for better dispersion of the catalytic materials. After that, it was cast on Torrey paper over a 1×1 cm^2 area, followed by proper vacuum drying of the modified electrode for 24 hours at 70 °C and used as a working electrode for HER applications.

4.3 Results and discussion:

Structural analysis:

XRD has been used primarily to probe the crystal structures, composite formation, and phases of as-synthesized samples. The diffraction peaks in NFS (Figure 4.1(a)) are well-matched with the rhombohedral phase. All the diffraction peaks found in the XRD of NFS validate the formation of a single phase that belongs to the H-M space group '$R\bar{3}c$'. To confirm the rhombohedral phase formation of the as-prepared NFS samples, we matched their XRD profile by integrated intensity refinement using FullProf.2k software. As shown in Figure 4.1(a), the simulated pattern is well-fitted with the experimental XRD pattern, and thus the formation of the pure rhombohedral phase in the as-prepared NFS sample is confirmed. The structural information like lattice parameters, lattice volume, and the goodness of the Le Bail fitting parameters are concise in Table 4.1. The Le Bail profile fitting agrees that the as-synthesized NFS did not expose any extra diffraction peak other than the rhombohedral phase. In NFS, $(SO_4)^{2-}$ and $(PO_4)^{3-}$ tetrahedra randomly share the corners of (FeO_6) octahedra to form the host unit.

Further, six of these host units bridge together, creating sizeable interstitial space that can easily harbor Na ions [171]. The average crystallite size of the material is found to be 41.72 nm using the Debye-Scherrer formula, while an almost similar result was found from the W-H plot ~78.13 nm. As shown in Figure 4.1(b), PPy shows a purely amorphous type diffraction pattern, while with increasing NFS loading, some diffraction peaks start appearing over the broad amorphous PPy-background. Owing to the high scattering factor of NFS particles, most of the characteristic diffraction peaks of NFS are found in the PPy/NFS-2%, which evidenced the formation of the PPy/NFS composite.

Table 4.1: Structural parameters for NFS

Structural parameters	a (Å); b (Å); c (Å)	Volume (nm^3)	α(°); β(°); γ(°)	R_p; R_{wp}; R_{exp}	Goodness of fit indicator, S	χ^2	Average crystallite size (nm)	
							Debye-Scherrer	W-H Plot
NFS	8.46836 8.46836 21.96642	1.575	90.0 90.0 120.0	11.6; 15.5; 7.94	1.95	3.8	41.72	78.13

Table 4.2: The functional group details analyzed from FTIR spectra

Peaks of the functional group present in PPy		
Peaks Positions (cm^{-1})	**Functional Groups in PPy**	**References**
617	N-N out of plane vibration	[172]
791	Ppy-ring bending	[172]
916	C-H out of plane deformation	[172]
1045	C-H in-plane (Ppy-ring) bending	[172]
1186	Breathing vibration of the pyrrole ring	[172]
1384	Fundamental vibrations of pyrrole ring	[172]
1465	C-N stretching vibration of pyrrole ring	[172]
1560	C═C stretch or C–C in-ring stretch	[172]
1630	C-C stretching in the pyrrole ring	[173]
3439	-OH stretching vibration	[173]
Peaks of the functional group present in NFS		
Peaks Positions (cm^{-1})	**Functional Groups in NFS**	**References**
500-750	O-P-O and O-S-O bending modes of vibration are present in PO_4^{3-} and SO_4^{2-}.	[171]
990	PO_4^{3-} symmetric/asymmetric stretching vibration	[171]
1049	SO_4^{2-} symmetric stretching vibration	[171]
1123	SO_4^{2-} asymmetric stretching vibration	[171]
3440	-OH stretching vibration band	[171]

Next, the molecular structure and functionality of the materials have been investigated through FTIR using KBr in transmittance mode, as shown in Figure 4.1(c). The peaks for pure PPy and NFS with different functional groups and moieties are depicted in Table 4.2, confirming the PPy polymer's formation. The presence of bending and stretching bands of the PO_4^{3-} and SO_4^{2-} units in the characteristics FTIR peaks of NFS also confirms the formation of NFS. In the case of composites derived from PPy and NFS, all the characteristic peaks are present along with some shifting in peak positions due to interaction between PPy polymer and NFS or may be due to changes in the environments of functional groups present, as depicted in Figure 4.1(c). It can also be seen that the intensity of some peaks varies as the amount of NFS varies in PPy/NFS composites.

TGA is one of the tools to investigate the thermal stability and quantification of the composition of individual components with different flame retardancy. Figure 4.1(d) shows the percentage weight loss of catalytic materials (here, we only considered PPy/NFS-5%, which shows the best catalytic activity towards HER) as a function of temperature. The plot also shows the weight loss at different stages to identify the degradation process. A slight weight loss in the range of 50 to 100 °C is observed at lower temperatures due to dehydration. The degradation of polymeric electrode materials starts after 200 °C and goes up to 450 °C with a weight loss of about 35%. Then, within the temperature range of 450 °C to 750 °C, the material's weight loss of about 54% can be attributed to the combustion process, which leads to a residual of about 5% in the case of PPy/NFS-5%. The same trend is seen in the case of pure PPy [174] with the residual of 2% of polymeric ash after 750 °C, while pure NFS is relatively thermally stable up to 700 °C, as can be seen from the TGA curve. Thus, PPy/NFS-5% shows slightly better thermal stability than pure PPy due to the presence of pure NFS.

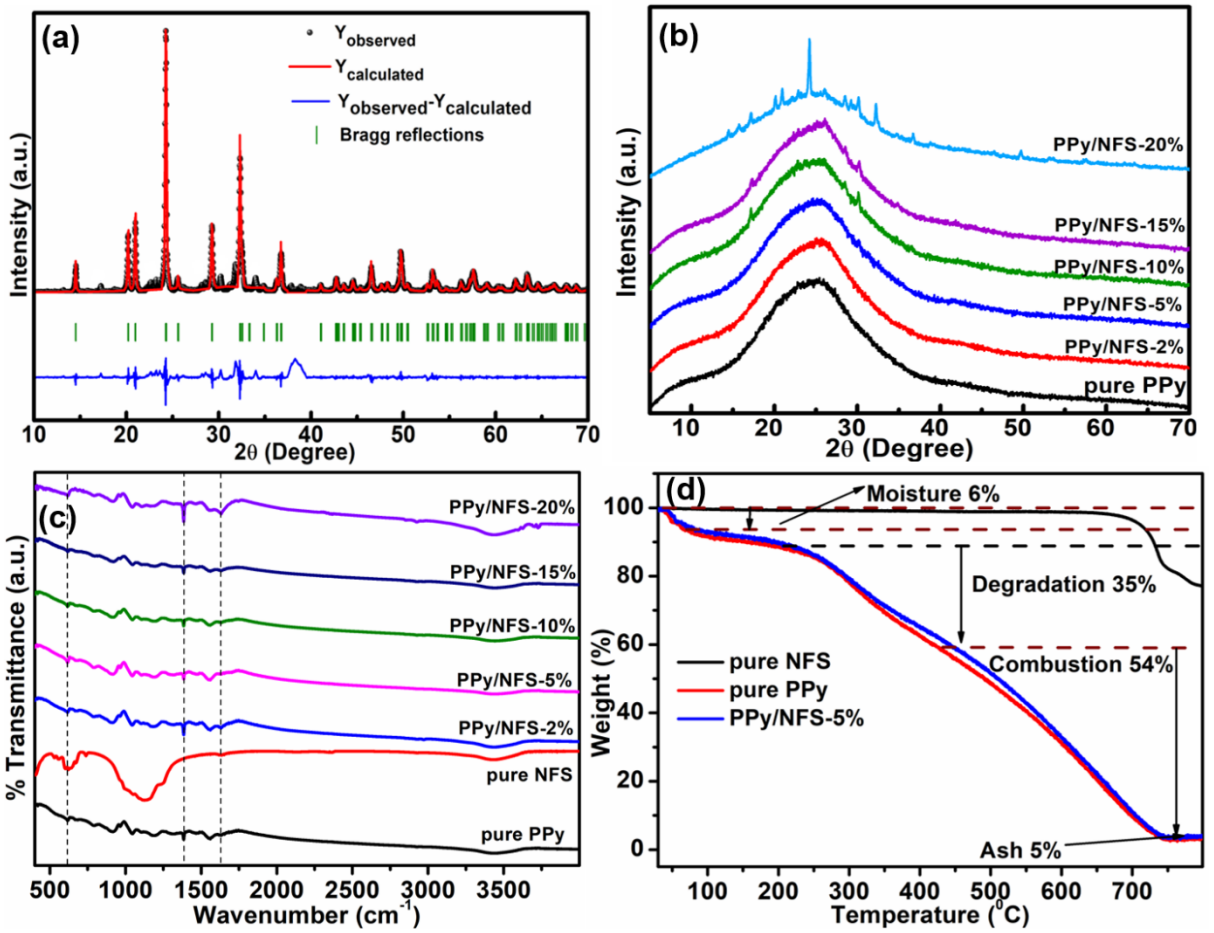

Figure 4.1: XRD of (a) Le Bail Profile fitting of the NFS XRD pattern, (b) XRD pattern of pure PPy and PPy/NFS composites, (c) FTIR spectra of pure PPy, pure NFS, and their composites, (d) TGA of pure PPy, pure NFS and PPy/NFS-5%.

The XPS spectra also confirmed the formation and composition of pure PPy, pure NFS, and PPy/NFS-5% composite materials. The peak survey of pure PPy is depicted in figure 4.2(a). The high-resolution deconvoluted peaks of C1s (figure 4.2(b)) show the association of four characteristic peaks corresponding to C-C at 285.2 eV, C=C at 284.1 eV, C-N at 288.2 eV of polypyrrole, and C=O at 286.6 eV due to oxidative polymerization [175]. The N1s XPS spectrum (Figure 4.2(c)) is deconvoluted in three peaks, counting imine nitrogen (-N=) at 399.8 eV, pyrrolic nitrogen (-NH-) at 400.4 eV, and charged nitrogen at 401.8 eV [175]. Figure 4.2(d) shows the XPS survey of pure NFS and the deconvoluted high-resolution peaks of its different elements are depicted in figure 4.2(e)-(i). The XPS spectrum of Fe2p at high resolution (Figure

4.2(f)) is split into two-part of Fe 2p3/2 (for Fe^{2+} at 711.5 eV) and Fe 2p1/2 (for Fe^{2+} at 725.4 eV) because of spin-orbit coupling [176]. The XPS spectrum of S2p (figure 4.2(g)) is split into two components S2p3/2 (B.E. 168.5 eV) and S2p1/2 (B.E. 169.3 eV) in sulfate environments [177]. The high-resolution XPS spectrum of O1s (figure 4.2(h)) observed for PO_4^{3-} at 530.6 eV, P=O/S=O at 531.1 eV, SO_4^{2-} at 531.8 eV and -OH 532.2 eV in pure NFS. The XPS spectrum of P2p (figure 4.2(i)) is also split into two components P2p3/2 (B.E. 132.9 eV) and P2p1/2 (B.E. 133.8 eV) in phosphate environments [176]. As depicted in figure 4.3(a), the XPS survey spectrum confirms the presence of all the individual elements C, N, O, Na, Fe, S, and P in PPy/NFS-5%. Figure 4.3(b) shows the high-resolution spectrum of C1s [175] in PPy/NFS-5% composite. The high-resolution spectrum of N1s [175] corresponding to the PPy/NFS-5% composite is shown in figure 4.3(c). The high-resolution spectrum of O1s (Figure 4.3(d)) observed mainly for $(PO_4)^{3-}$, $(SO_4)^{2-}$ presents in the NFS part of composites. The high-resolution spectrum of Na1s is shown in figure 4.3(e). The two parts of Fe2p (Figure 4.3(f)) of NFS ($Na_3Fe_2(SO_4)_2(PO_4)$) in PPy/NFS-5% exhibit two binding energy values each which are located at 709.7 eV and 724.5 eV for Fe^{+2} and 711.6 eV and 727.8 eV for to Fe^{+3} confirming the presence of +2 and +3 oxidation state of Fe [176], [177]. The +3-oxidation state of Fe in composites may be due to *In Situ* oxidative polymerization. The XPS spectrum of S2p [177] (Figure 4.3(g)) is like Fe2p, which splits into two components, S2p3/2 and S2p1/2, with binding energy values at 168.5 eV and 169.3 eV, respectively, corresponding to the environment of $(SO_4)^{2-}$. Similarly, the XPS spectrum of P2p [176] (Figure 4.3(h)) has two components, P2p3/2 and P2p1/2, with binding energy values at 132.8 eV and 133.7 eV, respectively corresponding to the $(PO_4)^{3-}$ environment present in NFS part of PPy/NFS-5% composites materials. It has been found from the above investigation that there is a shift in binding energy peak for N1s,

O1s and Fe2p in the case of composite PPy/NFS-5% from the pure PPy and pure NFS. This peak position shift can be attributed to the interaction between PPy and NFS.

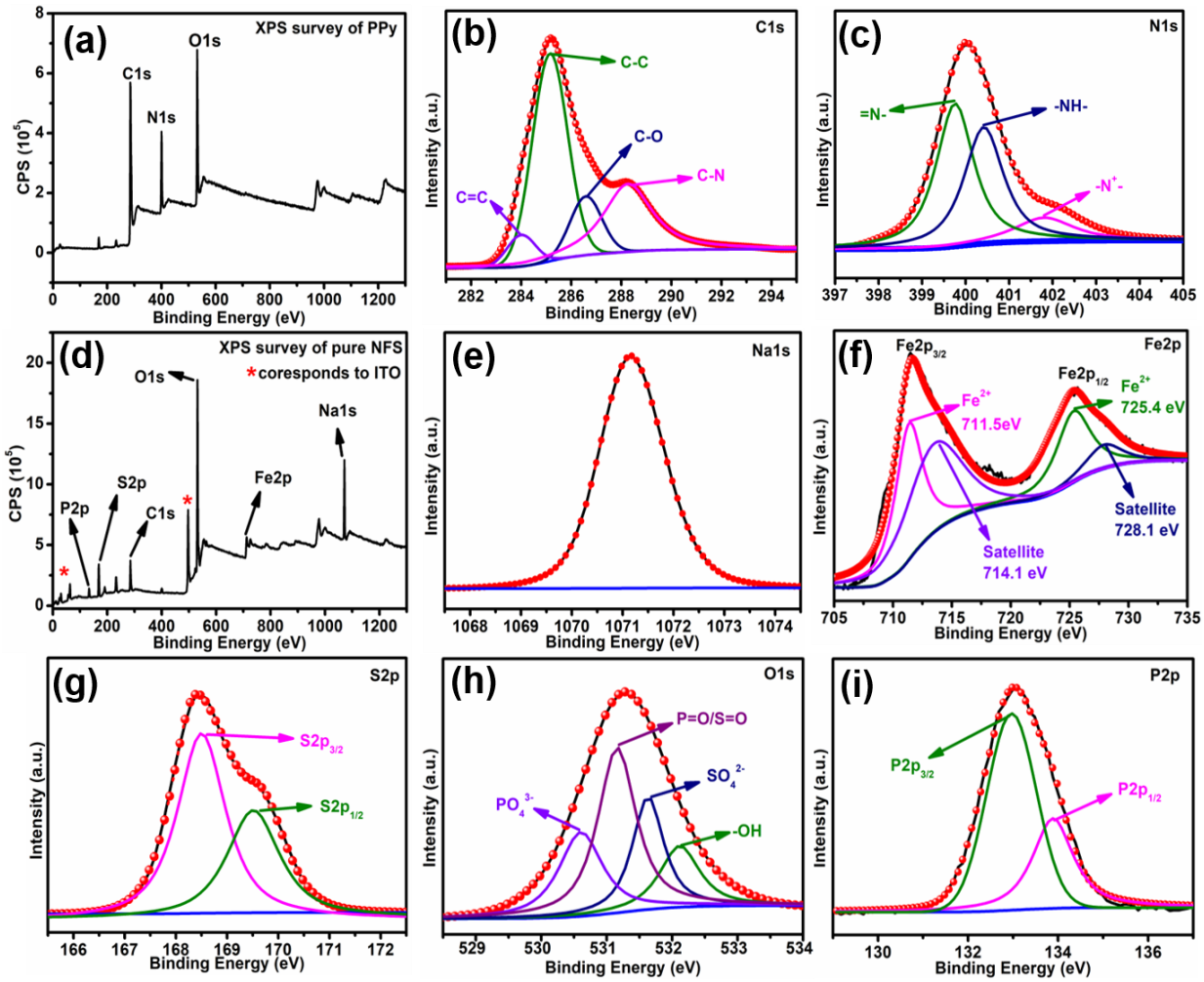

Figure 4.2: XPS spectra of (a) peak survey of pure PPy, Deconvoluted high-resolution XPS peaks of pure PPy, (b) C1s, (c) N1s, (d) peak survey of pure NFS, Deconvoluted high-resolution XPS peaks of pure NFS (e) Na1s, (f) Fe2p, (g) S2p and (h) O1s and (i) P2p.

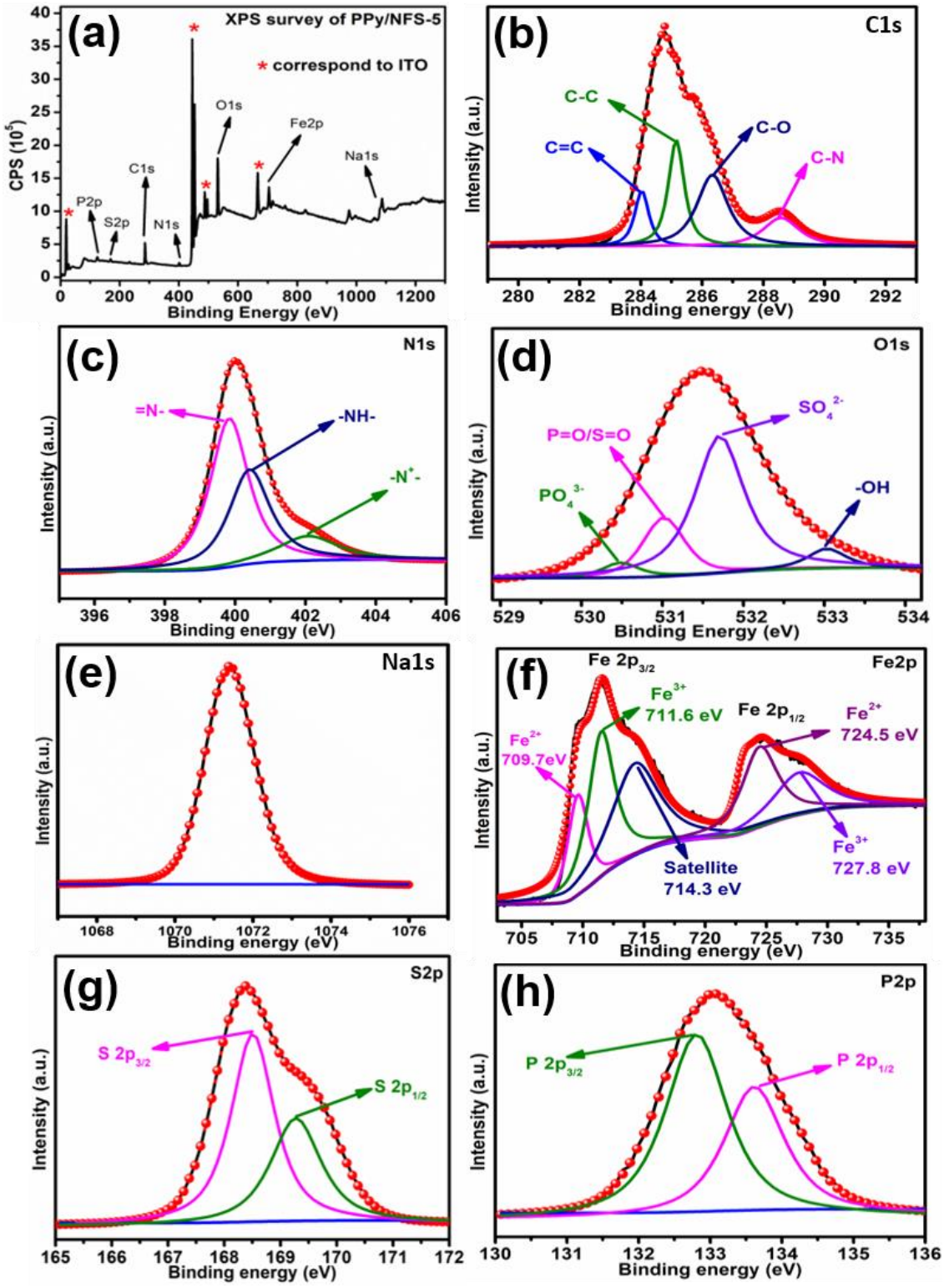

Figure 4.3: XPS spectra of PPy/NFS-5% (a) peak survey, high-resolution deconvoluted XPS peaks of (b) C1s, (c) N1s, (d) O1s, (e) Na1s, (f) Fe2p, (g) S2p and (h) P2p.

Surface Area Analysis:

Generally, the nature of catalytic materials like mass transport and electron transport abilities, dramatically depends on the porosity of catalytic materials. Therefore, to get more insight into the surface area of catalytic materials, BET and adsorption isotherm was performed to measure the surface area utilizing the N_2 adsorption-desorption isotherm at 77 K, as depicted in Figure 4.4. The improvement in the availability of active sites and the catalytic process can be made more efficient with a considerable increase in BET surface area [178]. In terms of shape and type, the catalyst materials exhibit type IV isotherm having a hysteresis loop that displays the mesoporous structure. At the relative pressure ($P/P_0 < 0.6$), the adsorption isotherm overlaps with the desorption isotherm, making it a reversible process for all three catalytic materials. Another discrete hysteresis loop can be seen in the higher range of *ca.* 0.6–1.0 P/P_0, with no overlapping between adsorption and desorption might also be attributed to the existence of a mesoporous structure of PPy/NFS-5%. The BET plot gives the specific surface area of 53.9 $m^2\ g^{-1}$, 6.03 $m^2 g^{-1,}$ and 177.8 $m^2\ g^{-1}$ for pure PPy (Figure 4.4(a)), pure NFS (Figure 4.4(b)), and PPy/NFS-5% (Figure 4.4(c)), respectively. These data reveal that the surface area of PPy/NFS-5% is 3.5 times larger than the individual pure PPy. It signifies that the presence of NFS in the PPy matrix enhances the surface area of composites by exfoliating the PPy, making it more porous, as depicted in Figure 4.4(c). The distribution of pore size of PPy/NFS-5% is determined using Brunauer-Joyner-Halenda (BJH) theory in the range of 10 to 60 nm, with the majority of pore size lying between 20 to 40 nm confirming the mesoporous features as shown in Figure 4.4(d). The pore volume of pure PPy is 1.239 $cm^3\ g^{-1}$, which increases to 4.084 $cm^3\ g^{-1}$ in PPy/NFS-5%, indicating a more exfoliated nature of PPy by the incorporation of NFS. Therefore, we concluded that incorporating NFS into the PPy leads to high porosity. This

porosity enhancement provides more active sites for interacting with ions which momentarily leads to a facile and faster electron movement for catalytic activity.

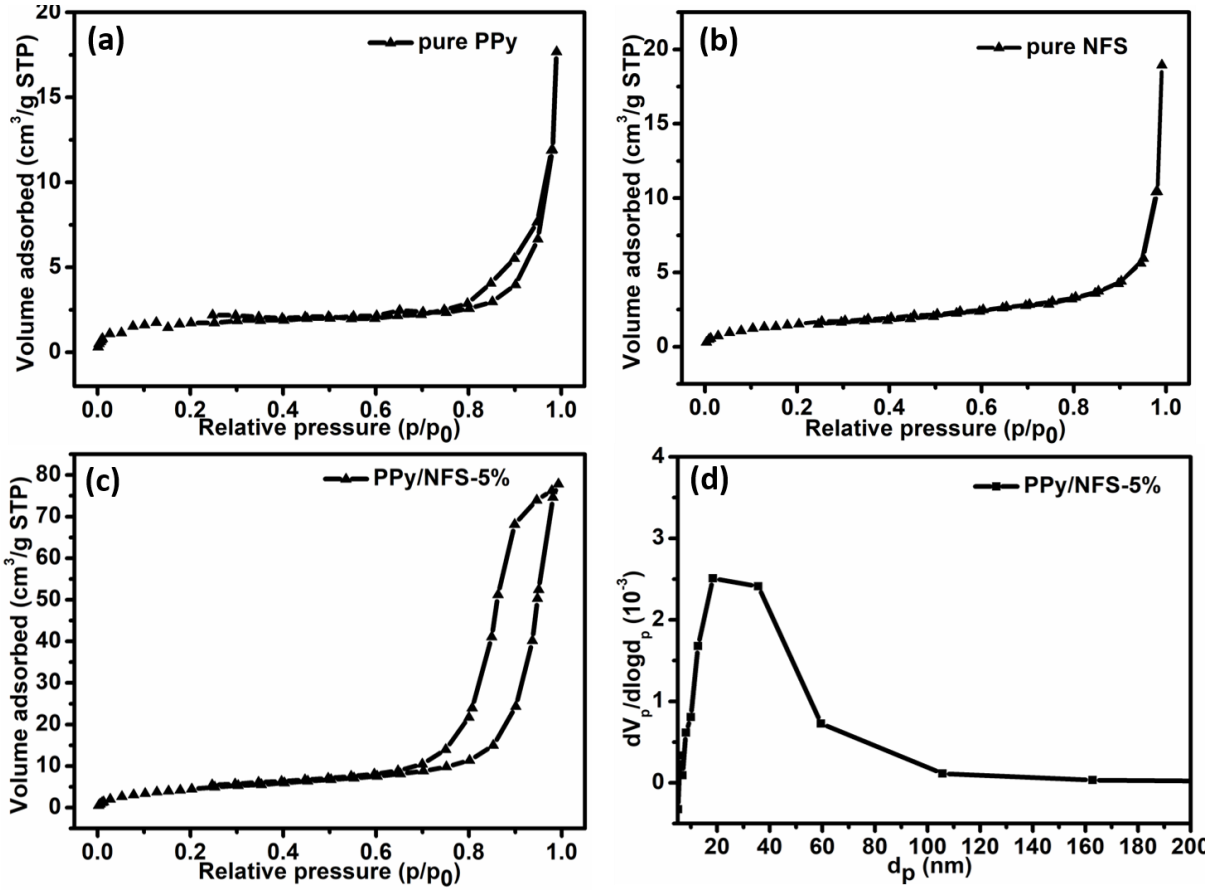

Figure 4.4: N_2 adsorption-desorption isotherm of (a) pure PPy, (b) pure NFS and (c) PPy/NFS-5%, (d) pore size distribution curve PPy/NFS-5%.

Morphological Analysis:

The SEM and TEM are used to explore the morphological analysis and composition of the catalytic materials, as displayed in Figure 5. The SEM image of pure PPy (Figure 4.5(a)) shows a uniform spherical morphology having an average diameter of ~300 nm. Figure 4.5(b) displays the SEM image of pure NFS, indicating granules-like morphology with different shapes and sizes. In the SEM image of the PPy/NFS-5% composite (Figure 4.5(c)), it can be seen that PPy

is more diffused with each other as well as with NFS, indicating some interactions between them. Also, the average spherical size of composite materials, PPy/NFS-5%, is smaller (~200 nm) than pure PPy, implying the availability of more active sites for catalytic activity. The TEM image of PPy/NFS-5% is shown in Figure 4.5(d). The TEM image also indicates the diffusion between PPy and NFS after composite formation. The NFS is well incorporated into the PPy matrix showing some sort of interaction (inset of figure 4.5(d)). This diffusion can also be related to XRD and XPS surveys. The EDAX in Figure 4.5(e) gives an idea of the different elements present in the composite materials. The uniform distribution of various elements of the filler part (i.e., pure NFS) into the catalytic composite materials, PPy/NFS-5%, is confirmed by mapping and depicted in Figure 4.5(f).

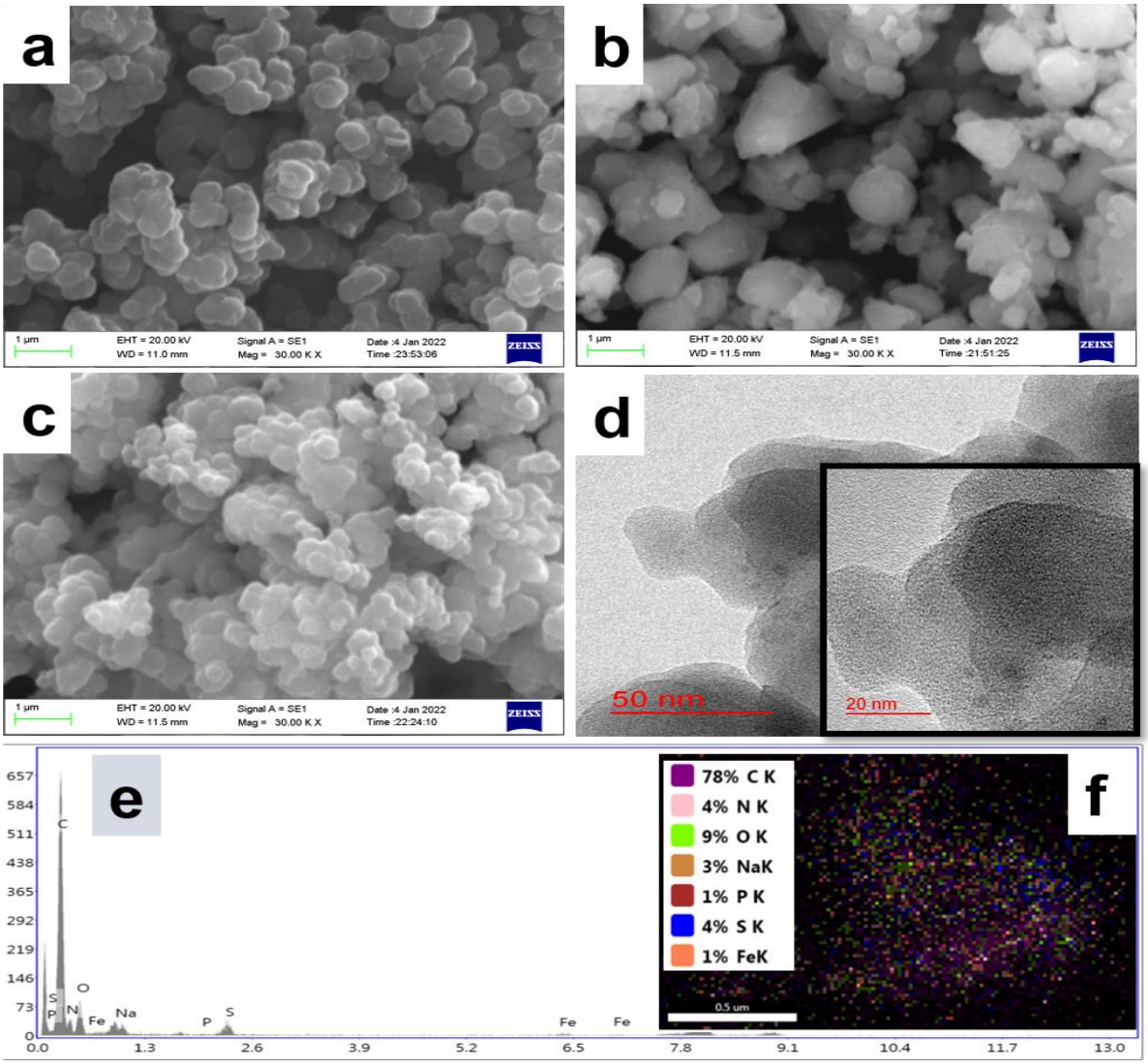

Figure 4.5: SEM images of (a) pure PPy, (b) pure NFS and (c) PPy/NFS-5%, (d) TEM image (inset shows the HR-TEM image), (e) EDAX, and (f) elemental mapping of PPy/NFS-5%.

Electrochemical Measurements:

The environmentally stable PPy polymer has good electrical conductivity among conducting polymers due to extended π-conjugation, but it shows poor HER activity. In the case of composites, the activity towards HER increases manifolds compared to pure PPy. The HER for different ratios of composite materials was characterized by electrochemical techniques LSV,

Tafel slope, and EIS, as shown in Figure 4.6. The LSV was done using a cathodic scan at 10 mV/s. The comparative hydrogen evolution for different electrode materials, including blank Torrey, pure PPy, pure NFS, and composites, is depicted by LSV in Figure 4.6(a). The PPy/NFS-5% shows the best catalytic activity for HER, as seen from the LSV curve in Figure 4.6(a). PPy/NFS-5% displays a lower onset overpotential of -26 mV vs. RHE than pristine PPy and NFS, whose onset overpotentials are -248 and -79 mV, respectively. It also shows a current density of 10 mA/cm^2 at a lower overpotential (η) of -206 mV as compared to other ratios of the composites materials. The onset overpotentials for other PPy/NFS composites ratios are -195 mV, -85 mV, -138 mV and -162 mV, corresponding to PPy/NFS-2%, PPy/NFS-10%, PPy/NFS-15% and PPy/NFS-20% respectively. The other ratios of the PPy/NFS composites show inferior catalytic activity than PPy/NFS-5% ratio, which is shown in Figure 4.6(a). The nitrogen in the PPy ring can easily interact with the metal center [164], [167], [170]. Due to the conjugation in PPy moieties, the electron sharing capability is enhanced from electron-rich nitrogen for PPy to NFS, which facilitates better charge transfer. Also, the PPy backbone contains positive charge centers, which also enhance charge transfer by interacting with the electron-rich centers. Because of these reasons, the effective active sites increase, facilitating easy hydrogen adsorption on the electroactive sites. This speed up the surface hydrogen coverage and hence larger HER probability. These reasons are optimal in the case of PPy/NFS-5% composite ratio and hence show better catalytic activity towards HER than other ratios due to optimized synergism between PPy and NFS. The HER performance based on PPy polymer is still less significant than Pt-based catalyst, but PPy/NFS-5% shows better and more efficient electrochemical activity. It also outperforms the majority of recently published PPy and other CP-based electrocatalysts in the HER, as depicted in Table 4.3.

Table 4.3: Comparison of HER performance of some recent polymer-based electrodes

S. No.	**Electrode materials**	**Electrolyte used**	**Onset potential (mV) vs. RHE**	**Overpotential at 10 mA/cm^2**	**References**
1	C|polyRu-MoS_x	0.5 M H_2SO_4	~ -300 mV	~ -400 mV	[179]
2	SiO2/PPyNTs–CFs	1.0 M NaH_2PO_4/Na_2HPO_4	-70 mV	~ -183 mV	[180]
3	PPy+MoS_2 Mix	0.5 M $HClO_4$	-0.4 V (SCE)	---	[181]
4	PPy/$ZnWO_4$	0.5 M H_2SO_4	---	-543 mV	[182]
5	PPy@SiO_2-HMS	1.00 M KOH	-61 mV	-123 mV	[164]
6	Co_3O_4/PPy/MWCNT	0.1 M KOH	-287 mV	-490 mV	[183]
7	$(Ppy/MoS_2)_{16}$-CC	0.5M H_2SO_4	-194 mV	-280 mV	[162]
8	Pt_{NPs}@MXene/PPy	0.5M H_2SO_4	---	-40 mV	[184]
9	PANI-Nbs	1 M KOH	-51 mV	-202 mV	[185]
10	PPy/NFS-5%	0.5 M H_2SO_4	-26 mV	-206 mV	This work

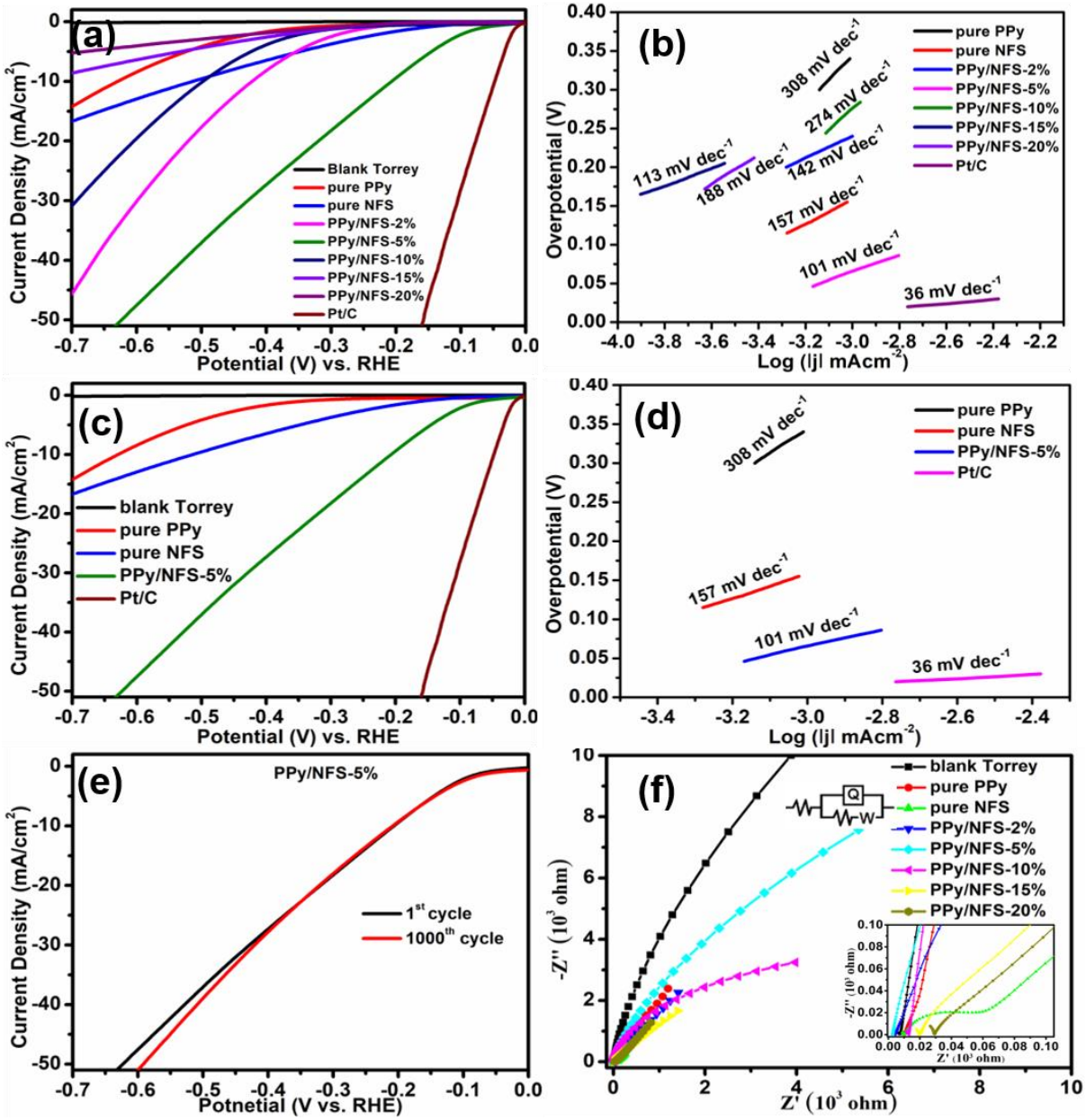

Figure 4.6: LSV curve of (a) all ratios of PPy/NFS composite materials, (c) PPy/NFS-5% with blank Torrey paper, Pt/C, pure PPy, and pure NFS. Tafel slope of (b) all PPy/NFS composite materials ratios, (d) PPy/NFS-5% with Pt/C, pure PPy, and pure NFS. (e) stability of LSV curve of PPy/NFS-5%. (f) EIS spectra of all PPy/NFS composites with blank Torrey, pure PPy, and pure NFS. All the measurements was done on carbon Torrey paper modified with catalytic materials having 1 cm^2 area.

Due to the fact that so much energy is required to produce activity and vice versa, a high Tafel slope implies large bandgap energy, resulting in a high overpotential. The LSV curve is utilized to calculate the Tafel slope using the Tafel equation i.e., $\eta = a + b \log (J/J_0)$; where the Tafel slope is denoted by "b" and current density by "J". An excellent catalytic activity towards HER in attributed by the lower value of Tafel slope [179], [181]. Our as-synthesized PPy/NFS-5% shows a lesser Tafel slope of 101 mV dec^{-1} compared to other PPy/NFS composites ratios, whereas 20% Pt/C displays a Tafel slope of 36 mV dec^{-1}. The Tafel slope of other ratios of PPy/NFS composites shows 142 mV dec-1, 274 mv dec^{-1}, 113 mv dec^{-1} and 188 mv dec^{-1} corresponding to PPy/NFS-2%, PPy/NFS-10%, PPy/NFS-15% and PPy/NFS-20% as depicted in Figure 4.6(b). The lower onset overpotential and Tafel slope in the PPy/NFS-5% make it a better electrode material for HER with high activity than other ratios. The Tafel slope for three limiting reactions for HER is derived using the Butler-Volmer equation. Electrolyte pH variations can affect the multistep HER process that occurs at the cathode. The intrinsic feature of catalysts affects the reaction's rate-determining step. After hydrogen adsorption (Volmer step), either electrochemical (Heyrovsky step) or chemical hydrogen desorption occurs in acidic solutions (Tafel step). The following pathways can be used to describe the HER process in the acidic medium: [62], [186], [187]

$$H^+ + e^- \rightarrow H_{ads} \qquad \text{(Volmer reaction)} \qquad \text{(eq. 4.1)}$$

$$H^+ + e^- + H_{ads} \rightarrow H_2 \qquad \text{(Heyrovsky reaction)} \qquad \text{(eq. 4.2)}$$

$$2H_{ads} \rightarrow H_2 \qquad \text{(Tafel reaction)} \qquad \text{(eq. 4.3)}$$

where H_{ads} is the adsorbed hydrogen on the catalyst's active sites. The HER may follow the Volmer-Heyrovsky or Volmer-Tafel pathway in any medium. In our situation, the PPy/NFS-5% follows Volmer-Heyrovsky-dominated routes in the HER process from the catalyst surface,

as indicated by a Tafel slope value of 101 mV dec^{-1}. No matter the path, the reaction always goes through the hydrogen atoms that have been adsorbed to the catalyst's surface. Therefore, Gibbs free energy (ΔG_{Had}) [188] for hydrogen adsorption plays a vital role in HER kinetics. Pt exhibits the best HER catalytic activity because it has a hydrogen adsorption-free energy value close to zero. A too-negative value for ΔG_{Had} can stop hydrogen molecule evolution by restricting the Tafel or Heyrovsky steps. Alternatively, if the ΔG_{Had} value is excessively positive, it becomes difficult to produce intermediate hydrogen, which slows down the Volmer step. Therefore, the optimal ($\Delta G_{Had} \sim 0$) hydrogen intermediate bonding energy for an HER catalyst should be such that hydrogen atoms are bound neither too loosely nor too tightly [62], [187], [188]. Due to the optimal synergistic effect between PPy and NFS, the value of ΔG_{Had} shifted close to zero in the case of PPy/NFS-5% composite, causing a faster rate of adsorption-desorption of hydrogen on the catalyst's active sites and hence better HER catalytic activity. Figure 4.6(c) depicts the LSV curve of pure PPy, pure NFS, and PPy/NFS-5% along with Pt/C for comparison, and its corresponding Tafel plot is depicted in Figure 4.6(d). The catalytic stability of PPy/NFS-5% was investigated by repeating the cycle of CV up to 1000 times, as shown in Figure 4.6(e). The PPy/NFS-5% has been found to have excellent catalytic stability toward HER.

The EIS technique is a handy tool to investigate mechanical aspects of the nanostructure of the various electrode materials and the ease of charge transfer through catalytic materials. The typical Nyquist plot of different catalytic materials in 0.5 M H_2SO_4 is depicted in Figure 4.6(f). The EIS measurement was performed at the onset potential for each electrode material from 10^5 Hz to 0.01 Hz of the frequency range. From Figure 4.6(f), the impedance curve for each electrode has an incomplete semicircle corresponding to the high-frequency area and a vertically inclined line associated with the low-frequency region. The diameter corresponds to

charge transfer resistance (R_{ct}) between the electrode and electrolyte. The intersection of the incomplete semicircle in the high-frequency zone on the real axis produces solution resistance (R_s) [182], [189]. The impedance data for different electrodes were analyzed and fitted with ZSimpWin 3.21 software using the circuit given in Figure 4.6(f) inset. As shown in Figure 4.6(f), the solution (electrolyte) resistance (R_s) is ca. 5-25 Ω. The charge transfer resistance (R_{ct}) for various electrode materials corresponding to pure PPy, pure NFS, PPy/NFS-2%, PPy/NFS-5%, PPy/NFS-10%, PPy/NFS-15% and PPy/NFS-20% are 3887 Ω, 33.53 Ω, 157.4 Ω, 28.85 Ω, 1142 Ω, 2036 Ω and 3850 Ω respectively. As seen from the data, the electrode materials PPy/NFS-5% show less resistance and provide easier admittance for intercalation and de-intercalation of charge compared to other ratios (compositions) of electrode materials. The denser and more compact structure might be a reason for preventing ions from migrating into the electrode materials.

The HER catalytic activity of the PPy/NFS-5% composite materials is also investigated at different scan rates to optimize the scan rate-dependent activity (figure 4.7(a)). PPy/NFS-5% shows better catalytic activity toward HER at a scan rate of 10 mV/s having almost the same onset overpotential. The diffusion-controlled process may be responsible for the variation in the LSV curve with different scan rates [187], [188]. The catalytic activity of PPy/NFS-5% is also investigated in different electrolytic mediums (figure 4.7(b)), i.e., 0.5 M Na_2SO_4 (neutral medium) and 0.5 M KOH (basic medium) along with acidic medium (0.5 M H_2SO_4). It has been found that the composite materials show better catalytic activity toward HER in an acidic medium which is in accordance with the semicircle of H_2 production. The environmental stability of the as-synthesized PPy/NFS-5% catalytic materials is tested after one year using LSV measurements (figure 4.7(c)). The long-term stability of the catalytic material PPy/NFS-5% was also investigated using chronoamperometric measurement for more than 50000

seconds at an overpotential of 206 mV vs. RHE (figure 4.7(d)). Figures 4.7(c) and 4.7(d) conclude that PPy/NFS-5% composite materials offer remarkable long-term catalytic and environmental stability and excellent durability.

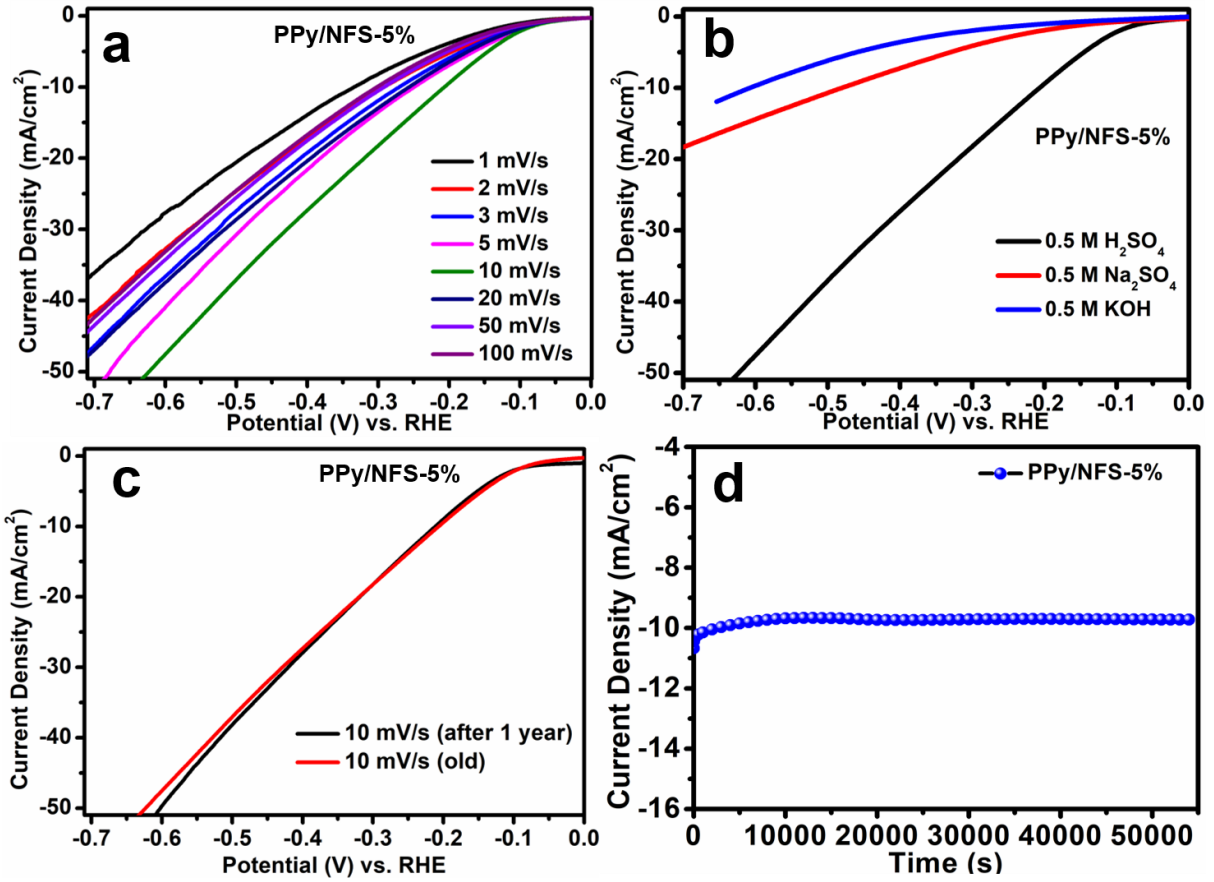

Figure 4.7: (a) LSV polarization curve at different scan rates, (b) LSV curve in the different medium at a scan rate of 10 mV/s, (c) LSV curve comparison for environmental stability and (d) Chronoamperometry curve for the long-term stability of PPy/NFS-5% in 0.5 M H_2SO_4.

4.4 Conclusion

In summary, pure PPy, pure NFS, and their composites were synthesized by chemical polymerization. XRD analysis confirms the rhombohedral phase of NFS and PPy/NFS composites. FTIR investigation confirms the different functional groups present in individual and composite materials. SEM and TEM images, EDAX, and mapping ensure the excellent incorporation of NFS into the PPy matrix. Improved electrical conductivity, synergism between PPy and NFS, large surface area, and porosity due to the integration of NFS into the PPy matrix are all factors that contribute to the composite materials' increased electrocatalytic activity towards HER. Among all the ratios of PPy/NFS, the PPy/NFS-5% ratio shows better HER activity with a lower onset potential of -26 mV and a current density of 10 mA/cm^2 corresponding to an overpotential of -206 mV. The Tafel slope of PPy/NFS-5% is 101 mV dec^{-1} which is lower than pure PPy, pure NFS, and other composites ratios. The as-synthesized PPy/NFS-5% offers good stability and excellent durability in electrocatalytic HER. The electrochemical results suggest that PPy/NFS-5% composites are a promising candidate for electrocatalytic hydrogen evolution reactions.